Springer

Acta Mechanica Sinica

CrossMark click for updates

• RESEARCH PAPER •

Acta Mech. Sin., Vol. 39, 322344 (2023)
https://doi.org/10.1007/s10409-022-22344-x

Transient heat transfer characteristics in spray cooling

Kewei Dong[1,2,3†], Di Wu[2†], Li Duan[2,3], Qi Kang[2,3], Jia Wang[2*], Jianlin Liu[1*], Zhiwei Wang[4], and Longsheng Duan[4*]

[1] *College of Pipeline and Civil Engineering, China University of Petroleum (East China), Qingdao 266580, China;*
[2] *Key Laboratory of Microgravity, Institute of Mechanics, Chinese Academy of Sciences, Beijing 100190, China;*
[3] *School of Engineering Sciences, University of Chinese Academy of Sciences, Beijing 100049, China;*
[4] *Beijing System Design Institute of the Electro-Mechanic Engineering, Beijing 100039, China*

Received October 22, 2022; accepted October 26, 2022; published online December 22, 2022

An experimental system of swirl spray cooling is designed to study the transient heat transfer efficiency of spray cooling with spray flow evolution. At an initial temperature of 300 °C, the spray cooling process is observed on a hot wall using a 20 mm × 20 mm square of aluminum alloy as the cooled specimen and water as the cooling medium. To measure the temperature variation, five high-precision thermocouples are used at five different locations along the vertical axis of the cooling specimen. Using the finite difference method, the one-dimensional unsteady heat conduction equation is solved, and the surface heat flux curve is obtained by inversion. The transient heat flux evolution curves under different working conditions are found by varying the spray height and flow rate. As a result, the spray cooling process is divided into four stages: I. the Leidenfrost effect stage (where the heat flux rises slowly), II. the liquid film formation stage (during which the heat flux rises sharply), III. the boiling stage (during which the heat flux decreases gradually), and IV. the convective evaporation stage (where the heat flux tends to equilibrium). As the heat flux reaches its peak value, the cooling process changes from the liquid film forming stage (stage II) to the boiling stage (stage III). The effect of spray height on liquid film is more significant when compared with the effect of pressure, which demonstrates that the heat transfer capacity at a spray height of 5 mm is significantly higher than at 10 mm and 15 mm, leading to the conclusion that the appropriate spray height is an important factor in maximizing the efficiency of spray cooling.

Citation: K. Dong, D. Wu, L. Duan, Q. Kang, J. Wang, J. Liu, Z. Wang, and L. Duan, Transient heat transfer characteristics in spray cooling, Acta Mech. Sin. **39**, 322344 (2023), https://doi.org/10.1007/s10409-022-22344-x

1. Introduction

Spray cooling is an active cooling method with a high heat transfer efficiency. It has the advantage of requiring less cooling medium and having a higher convective heat transfer coefficient than conventional cooling methods (such as forced air cooling, liquid cooling, and micro-channel cooling). For example, the critical heat flux (CHF) of spray cooling using water as the cooling working medium can reach 1000 W/cm^2 [1], while the CHF of pool boiling is approximately 120 W/cm^2. This means that the heat flux of spray cooling is roughly an order of magnitude higher than that of pool boiling. Spray cooling is considered as a key cooling technique for solving the problem of high heat flux.

The heat transfer mechanism of spray cooling is still unclear. However, the four most widely accepted heat transfer mechanisms of spray cooling include liquid film evaporation, forced convection, surface nucleation and secondary nucleation [2-4]. The CHF of spray cooling has a complex mechanism that is influenced by the physical properties of the working medium, structure of the cooling surface and the spray parameters. Estes et al. [5] proposed the CHF correlation model, which was based on volume flux and Sauter mean diameter, and accurately predicted the spray cooling performance of FC-72, FC-87 and water. Sodtke and Stephan [6] studied the spray cooling efficiency of

†These authors contributed equally to this work.
*Corresponding authors. E-mail addresses: wangjia@imech.ac.cn (Jia Wang); liujianlin@upc.edu.cn (Jianlin Liu); russellduanduan@163.com (Longsheng Duan)
Executive Editor: Xueming Shao

microstructure surfaces at different spray distances and found that microstructure surfaces outperform smooth surfaces in terms of cooling when subjected to the same wall superheat. Ravikumar et al. [7] confirmed that the use of dispersants increased the cooling rate of alumina nanofluids by 32.3%. Wang et al. [8] developed a generalized correlation equation between the local Nusselt number, spray Reynolds number, and dimensionless temperature in the non-boiling region of vertical and oblique spray. Cheng et al. [9] studied the effects of spray height, nozzle spray angle, inlet pressure, and spray incidence angle on spray cooling heat transfer, and confirmed that the parameters affect the heat transfer via modifying the flow field of the heating surface. Heat transfer performance can be improved by spraying at a lower spray height using a spray nozzle with a smaller spray angle and a higher inlet pressure. Fu et al. [10] have investigated the effect of spray angle on steel plate cooling, and discovered at 30°, the average cooling rate and heat flux increased by 22.1% and 11%, respectively, compared with at 0°. Hsieh et al. [11] determined the influence of mass flow rate Q, Weber number We, and degree of undercooling on the cooling capacity and efficiency of pure water and R134a working medium.

Previous research mainly focused on the steady-state heat transfer efficiency of spray cooling on heat source surfaces; however, there are few studies that examined the transient evolution of heat transfer mechanism during spray cooling relaxation process. Hsieh et al. [12] use optical visualization, heating surface views, and measurements of the evolution of liquid film thickness to determine the morphology and surface temperature distribution of transient impact droplets. Tian et al. [13] have proposed utilizing spray Biot number to characterize the ratio of internal thermal resistance of the cooling matrix to the convection heat transfer resistance of spray surface, and found that We is the key factor affecting surface heat transfer. Li et al. [14] studied the changes in spray morphology of propane, n-hexane and isooctane under transient boiling conditions. Cheng et al. [9] have observed the influence of different parameters on the spray flow field with a Doppler anemometer and camera. The experiments of Zhou et al. [15] showed that the film boiling zone took the longest time in the transient cooling process, and the time spent in the film boiling zone influenced the cooling rate in the transient process of spray cooling, where an increase in evaporation pressure can improve the cooling rate. At 750 K heating temperature, Ciofalo et al. [16] conducted cold water spray cooling on a thermos aluminum wall, and investigated the correlation between CHF, heat transfer coefficient, and spray parameters. In the convective heat transfer phase, Ebrahim et al. [17] developed an analytical model and accurately predicted the transient Nusslet number of free-falling droplets and air-propelled droplets moving over the surface. Tsukamoto et al. [18] discussed the effect of metal oxide on the cooling process during spray cooling and quenching at high temperatures. However, the transient heat transfer efficiency and its spray physical field evolution model have not been established yet.

The current understanding of the spray cooling is based on the heat transfer of steady-state. However, we found that many practical applications require rapid cooling from high temperature, for example, the thermal protection of high-speed aircraft, the quenching of metal materials, and the preparation of amorphous alloy. To our best knowledge, there is no systematic study on the transient efficiency of spray cooling. So this work aims to study the transient spray cooling, which goes through several stages, including the transition boiling, the nucleate boiling and evaporation. We have proposed a high-precision heat flux inversion method and compared the heat flux with the physical images of spray cooling. The inversion method appears a better sensitivity to the time-varying heat flux than the traditional heat estimation by thermal couples [19,20]. The experimental data are helpful to establish the relation between heat flow flux and spray flow pattern, which is of great significance for understanding the mechanism of spray cooling.

The transient heat transfer process of swirl nozzle spray cooling under different operating conditions is studied experimentally in order to assess the cooling process of heat flux transient evolution, and the heat flux curve is obtained in different stages. The heat transfer efficiency under instantaneous high heat flux density and the influence of multiple parameters on efficiency are analyzed, as well as the unsteady heat transfer evolution law of spray cooling. The experimental system and the experimental procedure are introduced in Sect. 2.1 and 2.2. In Sect. 2.3, the mathematical model of the cooled specimen is established based on the one-dimensional (1-D) heat conduction equation, and the heat flow inversion from the data of thermal couples is conducted by the finite difference method. Section 3.1 mainly shows the inversion of heat flow, which meets the law of energy conservation. In Sect. 3.2, four typical stages of the transient heat flow evolution of the transient process are analyzed. The effects of height and spray pressure on the maximum heat flux and the equilibrium heat transfer coefficient are discussed in Sect. 3.3 and 3.4. The systematic error of the experiment is analyzed in Sect. 4, and the conclusion is made in Sect. 5.

2. Experimental equipment and procedure

2.1 Experimental system

This experiment is to use a nozzle to atomize and spray the water droplets on the heated surface of the metal sample, as shown in Fig. 1. During the droplets collide to the metal

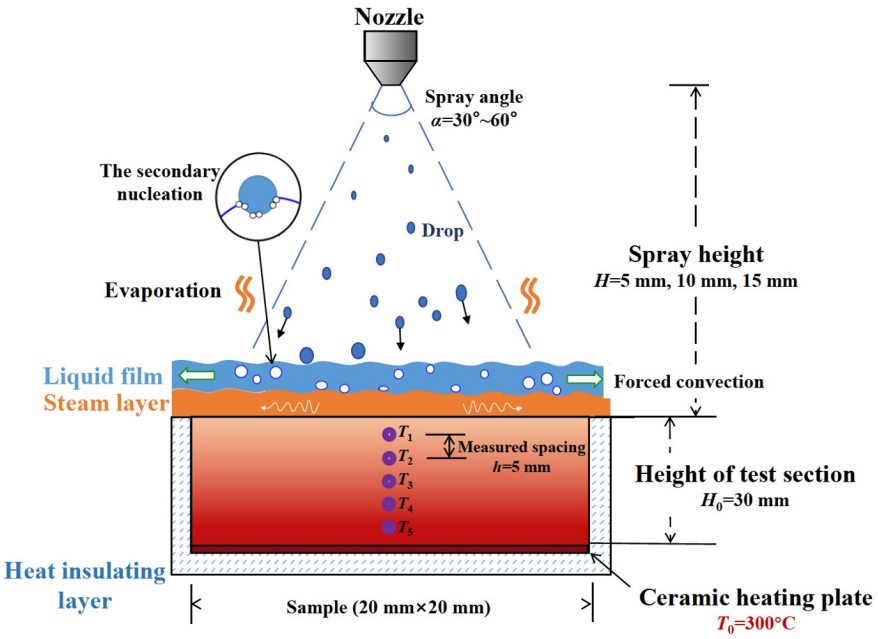

Figure 1 Heating model of experimental section.

surface, the heat is removed through the complex interaction between the droplets and the liquid film, such as evaporation, droplet bouncing, liquid film boiling, and secondary nucleation. To measure the heat flux of the spray cooling, five thermal couples are used to collect the temperature data during the cooling process. Meanwhile, a CCD camera is monitoring the spray flow to analyze the transient hydrodynamic mechanism of heat transfer.

The spray cooling experimental system consists of three parts: (1) liquid supply system; (2) experimental section and heating module; (3) data acquisition system as shown in Fig. 2.

The liquid supply system used high-pressure nitrogen as the initial pressure source and adjusted the pressure reduction valve to control the pressure P_{top} of the liquid storage tank. An air inlet and a liquid outlet were provided in the upper and lower parts of the liquid storage tank, respectively. Under the action of the pressure P_{top}, the liquid working medium flowed out of the liquid outlet of the liquid storage tank and enters the nozzle through the speed regulating valve. The high-pressure liquid is atomized, sprayed, and cooled on to the experimental surface via a nozzle. Using a collecting dish, the waste liquid was uniformly collected and treated. Two pressure transmitters (PCM300, made by Shenzhen Huibang) collected gas and liquid phase pressures, which were measured and controlled by a single circuit.

The experimental model consisted of two parts: a nozzle and a heating module. The pressure swirl atomizing nozzle is adopted produced by Geqiang Company, model: KCAE01, as shown in Fig. 3a. It was a hollow conical spray with a very small particle size, which was formed by friction and crushing of a high-speed rotating liquid film with air. The spray particle size was about 50-100 μm, the atomization cone angle was around 78°-98°, and the outlet diameter was 0.8 mm. The nozzle flow rate was shown in Fig. 3. The relation between the flow rate and pressure can be described by Bernoulli equation, and it can be obtained as

$$\Delta P = \frac{\rho Q^2}{2C_0^2 A_0^2}, \tag{1}$$

which the key parameters affecting nozzle flow Q included nozzle outlet pressure drop ΔP, fluid density ρ and nozzle outlet area A_0. The nozzle flow coefficient C_0 = 1.097.

The heating model comprises a heating plate, an insulation layer and an experimental model. The main body of the model was a 6061-aluminum alloy block of size 20 mm × 20 mm × 30 mm. Five K-type thermocouples (Nickel-chromium-Nickel-silicon, T_1-T_5) were spaced 5 mm apart in the direction H of the height of the experimental section. The thermocouple T_1 was located 5 mm beneath the cooled surface. The ceramic heating, which was placed at the bottom, heats the model with the heating power about 60 W. A Teflon insulation layer coated the model, preventing heat transfer along the vertical axis of the experimental section.

The data acquisition system was capable of synchronously acquiring high-precision thermocouple data and images of the cooling process, as well as observing the temperature and heat flux evolution process. The Agilent34972A data acquisition instrument was used to collect the temperature data from the 5-channel K-type thermocouple with a resolution of 22 bits and an experimental acquisition frequency of 1 Hz. Meanwhile, the camera captured the change

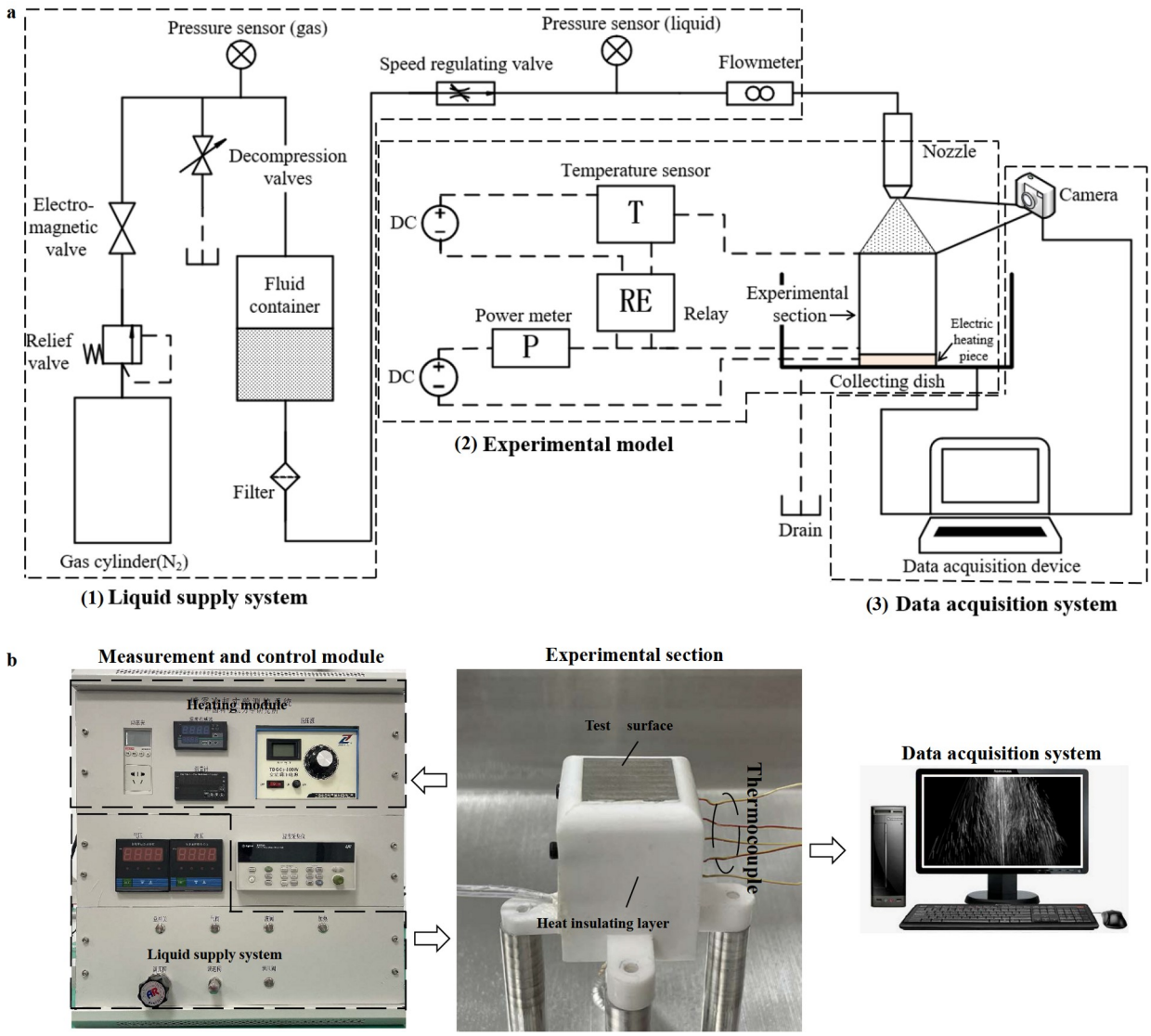

Figure 2 Experimental system schematic diagram and physical drawing: **a** schematic diagram of experimental system; **b** real picture of experimental system.

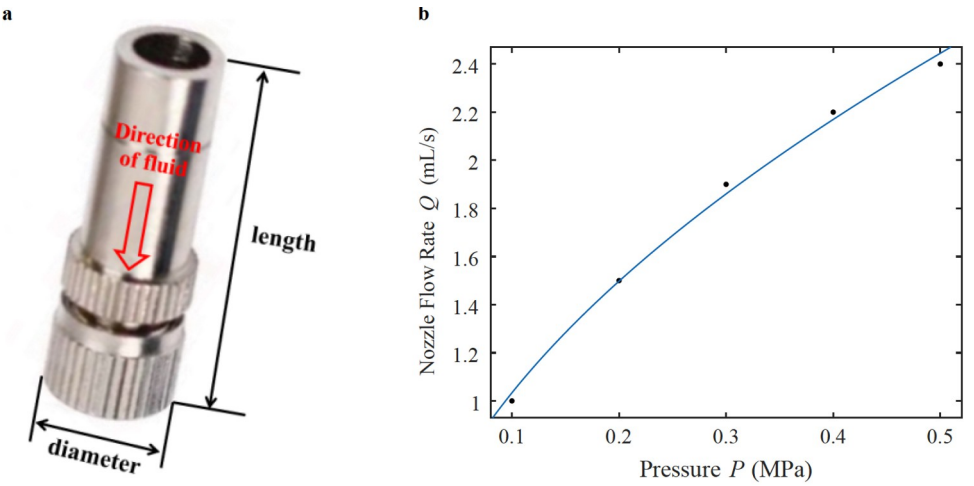

Figure 3 Nozzle physical drawing and measured nozzle flow parameters.

in liquid film morphology at the interface between spray and cooling.

2.2 Experimental procedure

The experiment was carried out as follows:

(1) Install the nozzle with a certain distance H_0 above the hot surface;

(2) Turn on the heating plate (U_0 = 60 V), and heat the specimen to T_0 = 300 °C;

(3) Record the temperature T_i (i = 1-5) of specimen, and start the camera to capture the images;

(4) Adjust the liquid pressure to P_0, then start the spray cooling process, and record the current working fluid flow Q;

(5) When the thermocouple temperature of each layer T_i (i = 1-5) changes ΔT_i by less than 1 °C in 5 min, it is regarded as experimental equilibrium and the experiment is ended.

The experiment studied the effect of different spray heights H_0 and working pressures P_0 on spray cooling efficiency. The working conditions are shown in Table 1.

2.3 Mathematical model

In the process of spray cooling, the experimental model can be regarded as a one-dimensional heat conduction problem in the vertical direction due to the upward heat flux generated by surface cooling, which satisfies the Fourier heat transfer equation:

$$\rho C\frac{\partial T}{\partial t}=\frac{\partial}{\partial z}\left(k(T)\frac{\partial T}{\partial z}\right)+q_l(z), \tag{2}$$

where z is the direction along the length of the test section, and $q_l(z)$ is the heat leakage from the side wall of the specimen. The heat leakage from the side wall can be neglected in the experiment because of the design of the insulating layer, that is to say $q_l(z)$ = 0. The specimen material is a 6061-aluminum alloy with a density ρ of 2800 kg/m^3 and specific heat capacity C of 896 J/(kg K). Since the temperature changes dramatically during the experiment, the effect of the temperature change on thermal conductivity k needs to be considered. The point laser heating method is used to measure the curve of the thermal conductivity of the 6061-aluminum alloy as a function of, as shown in Fig. 4.

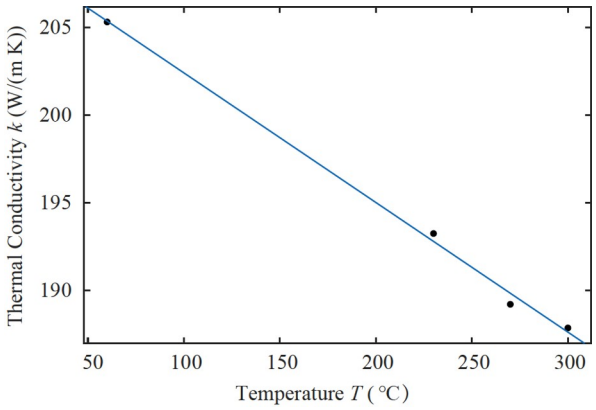

Figure 4 Variation curve of heat conduction coefficient k with temperature T.

There is a linear relationship between thermal conductivity k and temperature T, that is, k (T) = aT + b, a = −0.7566 W/(m K^2), b = 210 W/(m K).

Considering the linear relationship between thermal conductivity and temperature, Eq. (3) yields

$$\rho C\frac{\partial T}{\partial t}=(aT+b)\frac{\partial^2 T}{\partial z^2}+a\left(\frac{\partial T}{\partial z}\right)^2. \tag{3}$$

The heat flux boundary conditions on the upper surface of the specimen are as follows:

$$q_s=(aT+b)\frac{\partial T}{\partial z}\Big|_{z=0}=h(T_s-T_0). \tag{4}$$

The interfacial heat dissipation coefficient h is affected by many factors such as surface temperature, atomization conditions and phase change heat transfer. In the relaxation process of spray cooling, h is a function of time change. When the spray cooling reaches thermal equilibrium, h can be regarded as a constant. T_s is the temperature of the upper surface, while T_0 is the ambient temperature. Equation (3) indicates that the heat transfer on the upper surface of the specimen q_s can be obtained from the temperature gradient, which represents the heat transfer of spray cooling.

The heat flux boundary conditions on the lower surface of the specimen are as follows:

$$q_b=(aT+b)\frac{\partial T}{\partial z}\Big|_{z=-L}. \tag{5}$$

According to Eq. (5), heat transfer at the bottom of the specimen q_b can be obtained from the temperature gradient

Table 1 Experimental condition statistics

Spray height H_0 (mm) and working medium pressure P (MPa)								
No.	H	P	No.	H	P	No.	H	P
1		0.10	6		0.10	11		0.10
2		0.20	7		0.20	12		0.20
3	5	0.30	8	10	0.30	13	15	0.30
4		0.40	9		0.40	14		0.40
5		0.50	10		0.50	15		0.50

on the lower surface of the specimen, and the size of heat flux absorbed by the specimen from the heating plate can also be determined from the equation.

Transient heat flux on the upper surface is a key parameter in evaluating spray cooling efficiency. The surface heat flux estimation requires measuring the temperature values ($T_{1\text{-}5}$) from the thermocouple at z = 5 mm, 10 mm, 15 mm, 20 mm, 25 mm and extrapolating to the surface temperature gradient at z = 0 mm, 30 mm. In the relaxation process from the start of spray cooling to temperature equilibrium, the cooling specimen is in a non-equilibrium heat transfer process, and the temperature and heat flux exhibit a nonlinear distribution. In order to avoid the error caused by direct fitting, the difference method is used to numerically solve the heat conduction equation (2) in this paper. Combined with the measured values of $T_{1\text{-}5}$, the surface heat flux and temperature distribution change with time are determined using inversion. Experiments show that the heat flux inversion method combined with heat conduction equation offers improved accuracy and dynamic response.

The implicit central difference scheme is used to solve heat conduction. One dimensional spatial discrete grid $z_i = iL/N$, $i = N, N-1, ..., 0$, where L is the height of the cooling specimen, N = 300, and the time step Δt is 0.1 s. The temperature distribution of nodes is determined by column vectors $\mathbf{T} = (T^1, T^2, ..., T^N)^{\mathrm{T}}$. The difference matrix equation (3) is

$$\rho C\frac{\mathbf{T}_n}{\Delta t} = [k_{\mathrm{mat}}][D2]\mathbf{T}_n + a([D1]\mathbf{T}_n)^2 + \rho C\frac{\mathbf{T}_{n-1}}{\Delta t}, \tag{6}$$

where $[D1]$ is the first-order central difference matrix, and $[D2]$ is the second-order central difference matrix:

$$[D1]=\frac{N}{2L}\begin{bmatrix} -1 & 0 & 1 & & & & & \\ & -1 & 0 & 1 & & & & \\ & & & \ddots & & & & \\ & & & & -1 & 0 & 1 & \\ & & & & & -1 & 0 & 1 \end{bmatrix}_{(N-1)\times(N+1)}, \tag{7}$$

$$[D2] = \begin{bmatrix} 1 & -2 & 1 & & & & & \\ & 1 & -2 & 1 & & & & \\ & & & \ddots & & & & \\ & & & & 1 & -2 & 1 & \\ & & & & & 1 & -2 & 1 \end{bmatrix}_{(N-1)\times(N+1)}. \tag{8}$$

$\mathbf{T}_n$ represents the temperature column vector at the nth time step ($t = n\Delta t$). $\mathbf{T}_{n*}$ represents the estimated temperature vector at the nth time step. Each iteration time step advances to the nth time step through the temperature distribution of the $(n-1)$th time step. The difference iteration equation considering the heat flux boundary conditions is

$$\begin{bmatrix} \dfrac{K(T_{n*}^0)}{\Delta x} & \dfrac{-K(T_{n*}^0)}{\Delta x} & \cdots & \cdots \\ & \left(\dfrac{\rho C}{\Delta t}\mathbf{I}_n - [\mathbf{K}][D2]\right) & & \\ \cdots & \cdots & \dfrac{K(T_{n*}^n)}{\Delta x} & \dfrac{-K(T_{n*}^n)}{\Delta x} \end{bmatrix}\mathbf{T}_n$$

$$= \begin{bmatrix} q_n^{\mathrm{s}} \\ a([D1]\mathbf{T}_{n*})^2 + \rho C\dfrac{\mathbf{T}_{n-1}}{\Delta t} \\ q_n^{\mathrm{b}} \end{bmatrix}. \tag{9}$$

Each time step requires repeated iterations, and T_n of the last iteration is used as the estimated T_{n*} of the next iteration. When the convergence conditions, $|T_n - T_{n*}| < 10^{-6}$, are met, the current time step is completed, and the calculation for the next time step begins. The temperature distribution of each time step depends on the heat flux q_n^{s} and q_n^{b} of the upper and lower surfaces at that time. In order to perform an inverse analysis of the upper and lower surface heat flux, the values of the heat flux q_n^{s} and q_n^{b} are optimized to minimize the error between the simulation and experiment at the 5 measuring points, z = 5 mm, 10 mm, 15 mm, 20 mm, 25 mm.

When the upper surface heat flux is obtained, the interface heat dissipation coefficient h can also be calculated by Newton's law of cooling:

$$h = \frac{aT + b\partial T}{T_{\mathrm{S}} - T_0\partial z}\Big|_{z=0}. \tag{10}$$

According to the law of conservation of energy, the difference in heat flux between the upper and lower surfaces of the specimen is equal to the change in the total internal energy of the specimen:

$$\frac{\mathrm{d}U}{\mathrm{d}t} = mC\frac{\mathrm{d}\overline{T}}{\mathrm{d}t} = (q_{\mathrm{s}} - q_{\mathrm{b}})S, \tag{11}$$

where m is the overall mass of the test block, which is 0.0336 kg, and S is the cooling area. $\overline{T}$ is the average temperature of the specimen. Therefore, the accuracy and rationality of heat flux can be verified by energy conservation relation.

3. Results and discussion

3.1 Inversion of temperature distribution

In the initial stage of spray cooling, the sample temperature does not have a uniform gradient distribution due to two factors: the change in spray cooling mode and the unsteady heat transfer process of the cooled sample. Figure 5 shows the curve of temperature difference between adjacent thermocouples over time, using H = 5 mm and P = 0.3 MPa as

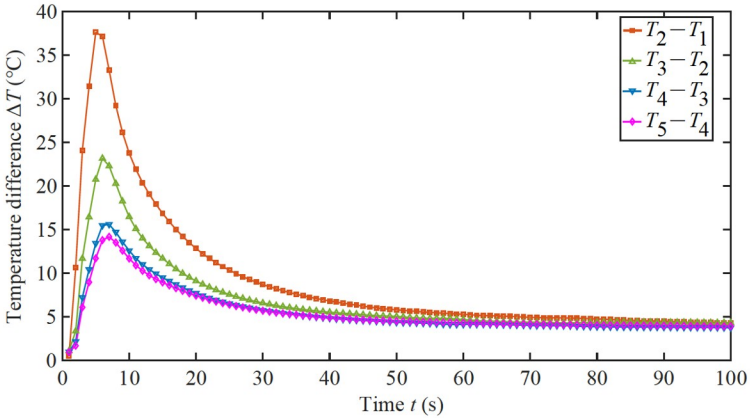

Figure 5 Temperature difference between thermocouples over time (H = 5 mm, P = 0.3 MPa).

an example. At the beginning of the cooling experiment, the temperature difference between the two thermocouples near the heat source surface, $\Delta T_{2,1} = T_2 - T_1$, is substantially greater than the temperature difference between the two thermocouples near the heating plate at the bottom of the experiment section, $\Delta T_{5,4} = T_5 - T_4$. Therefore, using average temperature to calculate the transient heat flux of spray cooling is not appropriate.

In order to precisely determine the dynamic heat transfer process of spray cooling, the temperature inversion method is utilized to get the temperature distribution in the specimen. Temperature inversion works on the following principle: the heat transfer process is numerically simulated using the heat conduction equation, and the temperature distribution changes with time under a specific heat flux density are obtained (Eq. (5)). The heat flux curve is optimized to minimize the error between the temperature distribution and the experimental data, yielding the temperature distribution and the surface heat flux. All the temperature values during the experimental period and during the cooling process can be obtained using this method, as shown in Fig. 6. Before starting spray cooling, the aluminum alloy specimen is close to the isothermal body, with temperatures of 300 at each point. Within 0-10 s after spray cooling has started, the temperature distribution presents a clear nonlinear curve, with a steep slope at the surface. This shows that the heat transfer efficiency of spray cooling is greater than the internal heat diffusion efficiency of the specimen, resulting in a nonlinear temperature distribution of internal heat and external cooling. At the end of the experiment, the temperature curve returns to a linear distribution, the surface heat transfer and heating power reach an equilibrium state, and the slope of the curve is proportional to the interface heat flux.

To verify the accuracy of the inversion results, the conservation of energy in the system is verified; that is, the difference in heat flux between the upper and lower surfaces of the specimen is equal to the reduction of internal energy (Eq. (10)). Figure 7 depicts the curves of the difference in heat flux between the upper and lower surfaces, as well as the decrease in internal energy over time when H = 5 mm and P = 0.3 MPa. In the initial stage of the test, there is a significant net heat flux that occurs within the first 0-10 s, reaching a peak of 986.5 W. Since the curves of internal energy change and net heat flux are consistent within the error range, the calculated results of heat flux are verified to be correct.

3.2 Heat flux evolution process

The experimental surface undergoes several physical processes from the Leidenfrost phenomenon or film boiling to nuclear boiling, and to evaporation, etc. It is important to discuss the change of heat transfer law at each stage. Figure 8 presents the typical heat flux curve of spray cooling and the evolution pattern of the spray flow process. The cooling evolution process can be divided into four stages (I-IV) based on cooling efficiency, liquid film shape, and experimental surface temperature.

Stage I (Leidenfrost effect stage): In the initial stage of cooling, the high temperature of the heat source surface induces the Leidenfrost effect; that is, when the liquid contacts the superheated surface, it exhibits non-wetting characteristics and forms a vapor layer between the heat source surface and the liquid. The movies show that the droplets bounce off the hot surface after the collision, and a liquid film is not formed yet on the surface of the heat source. The vapor layer between the droplet and the heat source surface evaporates, primarily facilitating heat transfer and cooling. The efficiency is extremely low, with a heat flux density q_{I} of less than 3.41 W cm^{-2} on the experimental surface.

Stage II (Liquid film formation stage): Obvious heat exchange occurs during droplets collision, which leads to a large amount of steam and a sharply increasing of the heat flux. Spray droplets penetrate through the vapor layer

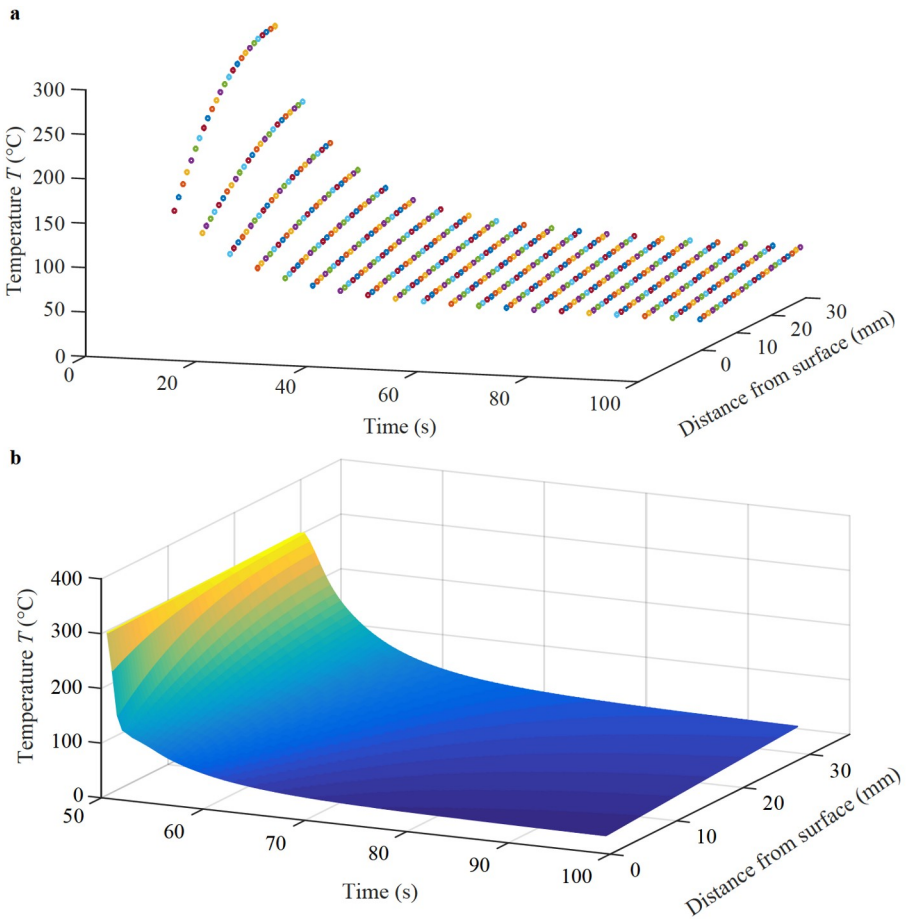

Figure 6 Temporal and spatial distribution of temperature in the experimental section (H = 5 mm, P = 0.3 MPa): **a** inverse scatter diagram; **b** inversion surface.

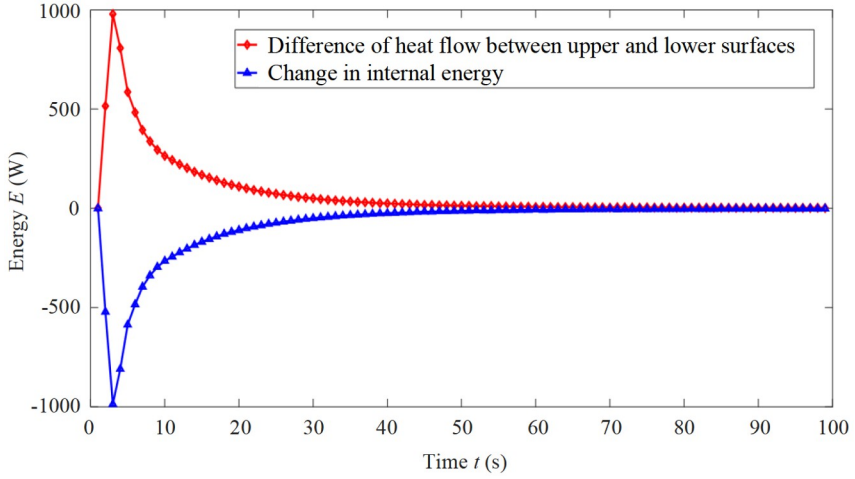

Figure 7 Verification of energy conservation of the system (H = 5 mm, P = 0.3 MPa).

formed by Leidenfrost effect and directly hit the heat source, immediately making contact and heat exchange with the surface. The heat flux rises to q_{II} = 244.68 W cm^{-2}, which is the highest value q_{max}, as the temperature of the experimental section falls. At this point, the liquid film has gradually formed.

Stage III (Boiling stage): The liquid film is formed and accumulated, and it gradually transitions from the transition boiling to nuclear boiling. On the surface of the heat source, the liquid film is annular. As the surface temperature decreases gradually during the cooling process, the heat flux decreases gradually, and the value of heat flux q_{III} at this

stage is 98.64-244.68 W cm^{-2}.

Stage IV (Convective evaporation stage): The criterion for this stage is that the surface temperature is less than the boiling point (100). The heat flux is caused by evaporative heat dissipation and the forced flow induced by spray impinges. The experimental section gradually tends to the thermal equilibrium state, in which the heat flux of the upper surface steadily dropped to match the heating power of the bottom surface. The final heat flux density (q_{IV}) in Fig. 8 is 14.40 W cm^{-2}, the heat flux is 57.6 W, and the heating power of the lower surface is 58 W at H = 5 mm, P = 0.3 MPa.

3.3 Parameter effect of peak heat flux

When the nozzle and cooling surface parameters are determined, the spray height H and working medium pressure P have the greatest influence on the peak heat flux. Spray coverage area and atomization properties are primarily affected by spray height, while working medium pressure affects working medium flow rate and spray speed. The effect of different spray height H and working medium pressure P on peak heat flux q_{max} is then discussed.

The experimental results show that the peak heat flux q_{max} of spray cooling increases with the decrease of height, as shown in Fig. 9. This is because the spray impingement is intensified as the height decreases, enhancing the CHF of spray cooling. When the height H reaches 15 mm, a part of the hollow cone spray exceeds the experimental surface. As the working medium pressure P increases, the peak heat flux q_{max} first decreases and then increases. When the height H = 10 mm, the spray covers most area of surface, and the peak heat flux q_{max} is enhanced if the pressure is increased. When the height H = 7.5 or 5 mm, the maximum heat flux is insensitive to the pressure, and the heat transfer efficiency seems to be saturated by the dense spray. The liquid film morphology under different working conditions is given in Fig. 10. It is observed that the larger distance H or the high pressure P lead to a thinner liquid film on the hot surface. It is because the spray under larger distance or high pressure can form a shearing flow near the edge of the surface, which drives the fluid to flow down from the specimen and reduces the liquid accumulation.

3.4 Influence of parameters on surface heat transfer coefficient

The surface heat transfer coefficient h represents the heat

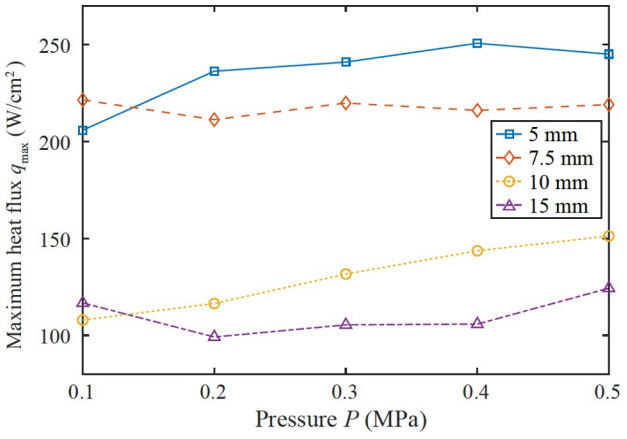

Figure 9 Influence of spray height and working medium pressure on peak heat flux.

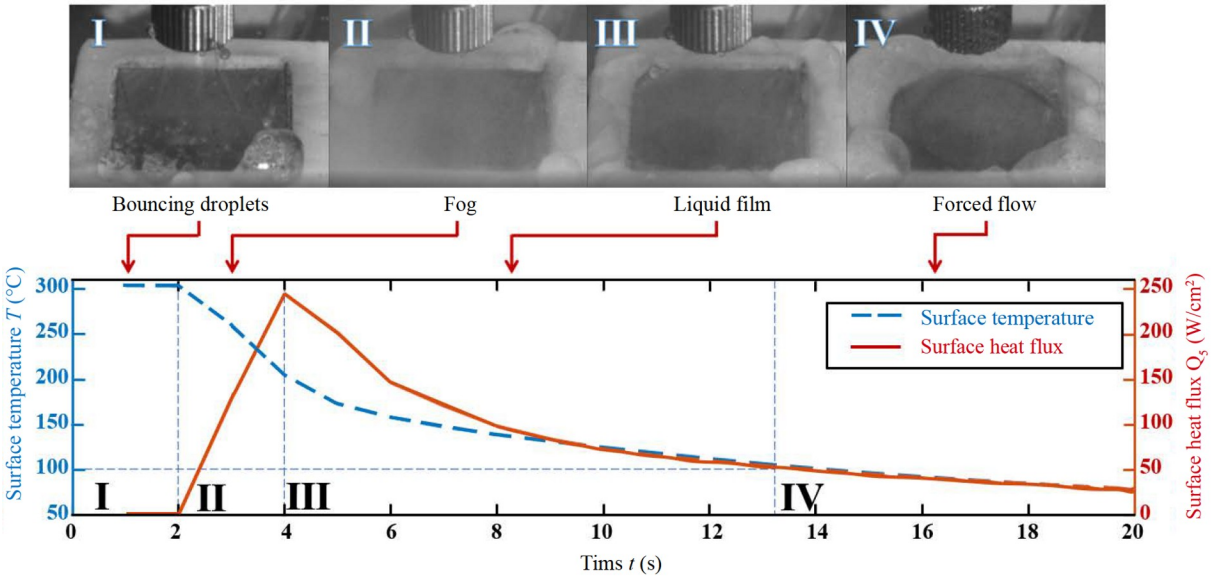

Figure 8 Influence of spray flow state on heat flow curve (H = 5 mm, P = 0.3 MPa, experimental surface temperature $T_I \geq 300$ °C, 200 °C $\leq T_{II} \leq 300$ °C, 100 °C $\leq T_{III} \leq 200$ °C, $T_{IV} \leq 100$ °C).

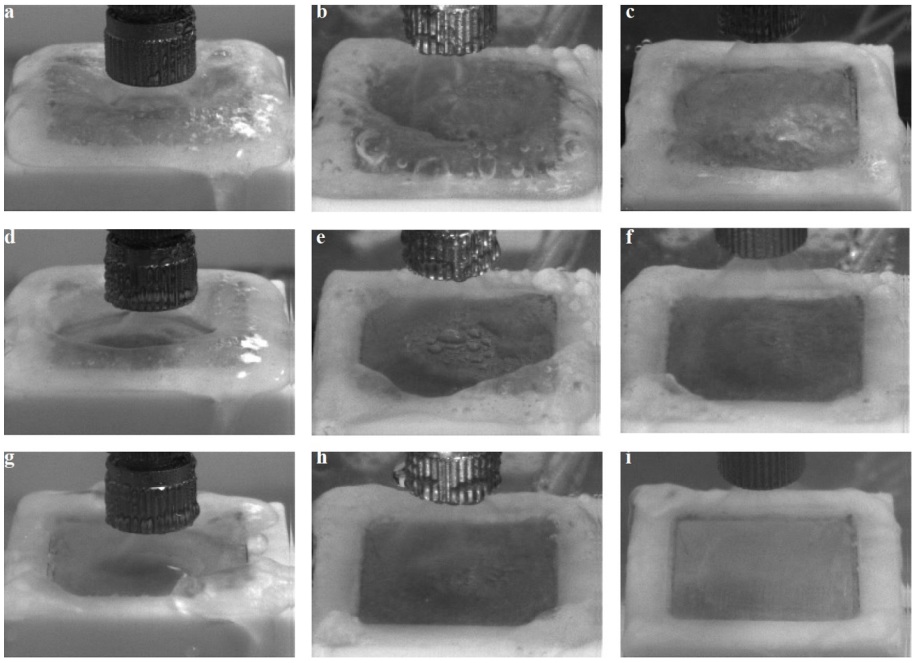

Figure 10 Comparison of liquid film morphology under different working conditions: **a** $H = 5$ mm, $P = 0.1$ MPa; **b** $H = 10$ mm, $P = 0.1$ MPa; **c** $H = 15$ mm, $P = 0.1$ MPa; **d** $H = 5$ mm, $P = 0.3$ MPa; **e** $H = 10$ mm, $P = 0.3$ MPa; **f** $H = 15$ mm, $P = 0.3$ MPa; **g** $H = 5$ mm, $P = 0.5$ MPa; **h** $H = 10$ mm, $P = 0.5$ MPa; **i** $H = 15$ mm, $P = 0.5$ MPa.

dissipation performance of spray at equilibrium. Under the rated heating voltage of 60 V, the influencing factors of spray heat transfer performance h can be studied by changing the spray height H and working medium pressure P.

The heat transfer coefficient h increases with the rising working medium pressure P, as shown in Fig. 11. As the distance H is decreasing, the enhancement of heat transfer coefficient h becomes more significant. When the cover range of spray is fully located inside the surface (H = 5 or 7.5 mm), the heat transfer coefficient h is increasing with the decrease of height H. The heat transfer coefficient increases with the increase of pressure or the decrease of distance, because the heat transfer coefficient is proportional to the tensity of the forced convection in the equilibrium state. When H = 10 or 15 mm, the increasing trend of the heat transfer coefficient is not apparent when the pressure P increases. The reason for this is that when the spray height H increases, the effect of the swirl nozzle causes a portion of the hollow cone spray to extend beyond the experimental surface, increasing size of the hollow area formed on the experimental surface. Figure 12 displays the 10 mm and 15 mm spray cooling images. The red dotted line represents the edge of the hollow area. It is obvious to observe that the hollow area increases as the height increases. When the working medium pressure P is low, the liquid film flows to the central region under the influence of gravity at the later stage of the cooling experiment, reducing the area of the central region. However, the obstruction effect of fog droplets on the flow of the liquid film to the central region is increased as the working medium pressure P gradually increases, making it impossible to further reduce the area of the central region and improve the heat transfer capacity.

4. Uncertainty analysis

Table 2 shows the accuracy of the measuring instrument for uncertainty analysis.

The error of heat flux q in the inversion process is mostly determined by the error of experimental temperature data.

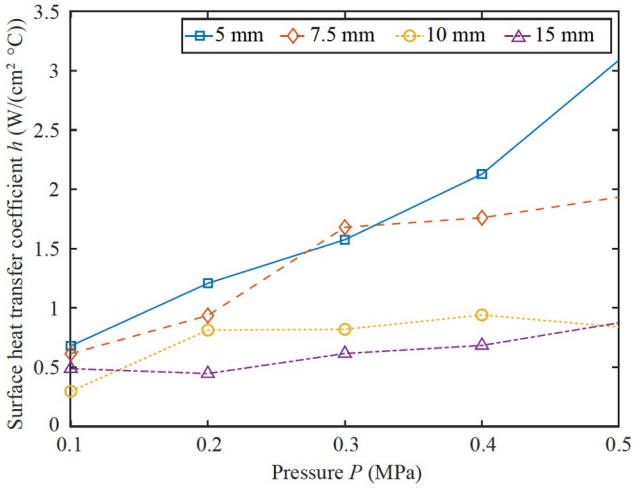

Figure 11 Influence of working medium pressure P on surface heat transfer coefficient h at different spray height H.

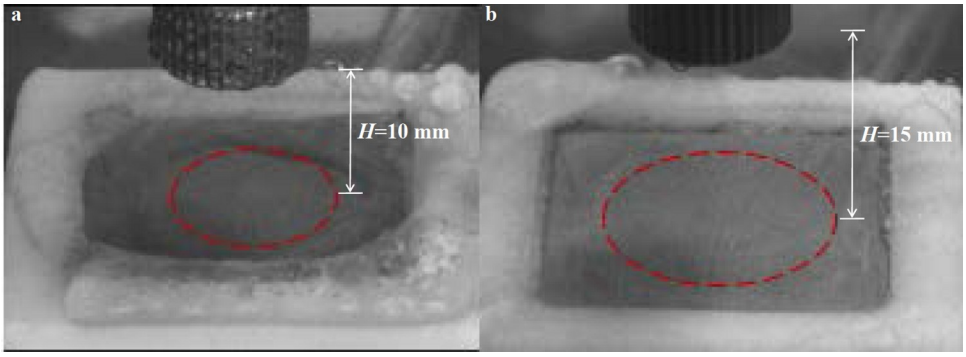

Figure 12 Comparison of 10mm and 15 mm hollow areas: **a** 10 mm height to form a hollow area; **b** 15 mm height to form a hollow area.

Table 2 The measurement errors of instruments

Measuring instrument	Range/Counting range	Measuring accuracy
Pressure sensor	0-1.6 MPa	0.5%
Single loop display measurement instrument	0-1000	0.5%
K-type thermocouple	−200 °C-1300 °C	±0.1 °C
Flowmeter	15-500 mL/min	0.5%

Due to the complexity of the error transfer function of heat flux q in the inversion algorithm, numerical experiments are required to estimate the error. We generate artificial data of the thermocouples by simulation, which is the temperature response of a standard impulse heat flux. And then we input the artificial data to our inversion algorithm, so that the error of heat flux inversion can be estimated by comparing the heat flux inversion q_{In} and the standard heat impulse q. To generate the artificial data near ideal experimental results, the thermal conduction equation is solved by the direct simulation for the given heat flux q. After that, to simulate the measurement error of the thermocouples, we add the Gaussian errors $N(\mu, \sigma)$, where the systematic error $\mu = 0$ and the root mean square $\sigma = 0.033$. Figure 13 shows the artificial data of thermocouples, and the corresponding standard heat flux is given in Fig. 14. Figure 14 shows the comparison of the standard heat flux impulse and the heat flux inversion from the artificial data. The maximum heat flux error is 2.9% in the whole experimental process.

5. Conclusion

In this paper, an experimental spray cooling platform is set up to investigate the transient heat transfer process of spray cooling under various operating conditions. The transient heat flux density curve evolves over time, revealing the correlation between the heat flux change process and the morphology of the spray and liquid film. In conclusion, the paper is summarized as follows.

(1) During the cooling process, the surface heat flux goes through four stages: I. leidenfrost effect stage (slowly rising), II. liquid film formation stage (sharp rise), III. boiling stage (gradual decline), and IV. convective evaporation stage (tend

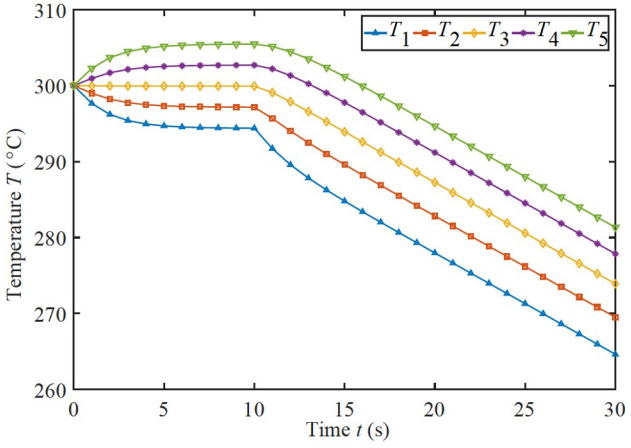

Figure 13 Simulated temperature distribution at sampling points in the experimental section.

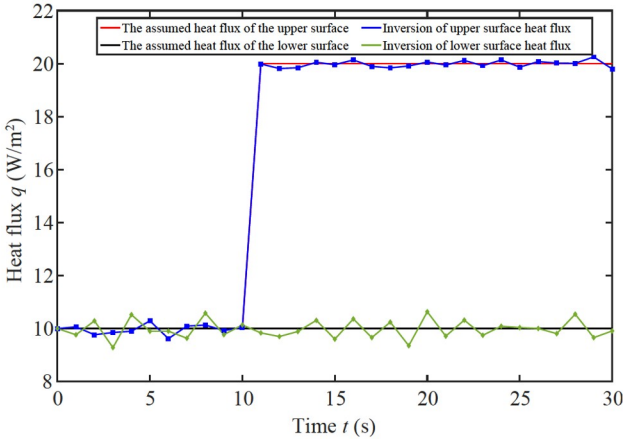

Figure 14 Assume that the given surface heat flow density is compared with the surface heat flow density after adding the error.

to equilibrium). In stage I, the droplet exhibits a non-infiltrating bounce phenomenon on the experimental surface with high superheat due to the Leidenfrost effect, and no liquid film is formed, resulting in a poor heat transfer effect. During the formation stage of the liquid film, the droplet particles vaporize intensely, producing a large volume of steam. As the liquid film forms gradually, the heat flux increases rapidly. In the boiling stage, the superheat of experimental surface decreases gradually, as does the heat flux. The surface temperature is lower than the boiling point during the convective evaporation stage, and the boiling phenomenon disappears as it gradually reaches equilibrium.

(2) The peak heat flux q_{max}, which is influenced by the working medium pressure P and spray height H, appears at the transition from stage to Stage . When the spray height H is 5 or 10 mm, the peak heat flux q_{max} increases as the working medium pressure P increases. Since the spray cone angle increases with increasing working medium pressure, the hollow area of the experimental surface increases, part of the spray exceeds the experimental surface, and the heat flux shows a certain downward trend when the spray height H = 15 mm.

(3) The heat transfer coefficient increases with the increase of pressure or the decrease of distance, because the heat transfer coefficient is proportional to the intensity of the forced convection in the equilibrium state. When the spray height is larger, the pressure has a limited influence on the surface heat transfer coefficient h. This is because increasing the pressure leads to an increase in the hollow spray cone angle, which caused a hollow area in the liquid film. Therefore, compared with the influence of the working medium pressure, spray height has a greater influence on the surface heat transfer coefficient h.

Author contributions *Longsheng Duan and Zhiwei Wang set out overall research objectives. Kewei Dong designed the research. Kewei Dong wrote the first draft of the manuscript. Kewei Dong set up the experiment set-up and processed the experiment data. Di Wu and Jia Wang helped organize the manuscript. Di Wu revised and edited the final version. Li Duan and Qi Kang provided financial support for the study. Jianlin Liu supervised the planning and execution of the research activities.*

Acknowledgements *This work was supported by the National Natural Science Foundation of China (Grant Nos. 12032020, 12072354 and 12102438), the Manned Space Program of China, the Strategic Priority Research Program on Space Science of Chinese Academy of Sciences, the Project funded by China Postdoctoral Science Foundation (Grant No. 2019M660812), and the Natural Science Foundation of Shandong Province (Grant No. ZR2018BA022).*

1 K. A. Estes, and I. Mudawar, Comparison of two-phase electronic cooling using free jets and sprays, J. Electron. Packag. **117**, 323 (1995).
2 R. P. Selvam, L. Lin, and R. Ponnappan, Direct simulation of spray cooling: Effect of vapor bubble growth and liquid droplet impact on heat transfer, Int. J. Heat Mass Transfer **49**, 4265 (2006).
3 E. A. Silk, E. L. Golliher, and R. Paneer Selvam, Spray cooling heat transfer: Technology overview and assessment of future challenges for micro-gravity application, Energy Convers. Manage. **49**, 453 (2008).
4 A. G. Pautsch, and T. A. Shedd, Spray impingement cooling with single- and multiple-nozzle arrays. Part I: Heat transfer data using FC-72, Int. J. Heat Mass Transfer **48**, 3167 (2005).
5 K. A. Estes, and I. Mudawar, Correlation of sauter mean diameter and critical heat flux for spray cooling of small surfaces, Int. J. Heat Mass Transfer **38**, 2985 (1995).
6 C. Sodtke, and P. Stephan, Spray cooling on micro structured surfaces, Int. J. Heat Mass Transfer **50**, 4089 (2007).
7 S. V. Ravikumar, K. Haldar, J. M. Jha, S. Chakraborty, I. Sarkar, S. K. Pal, and S. Chakraborty, Heat transfer enhancement using air-atomized spray cooling with water-Al_2O_3 nanofluid, Int. J. Thermal Sci. **96**, 85 (2015).
8 Y. Wang, M. Liu, D. Liu, K. Xu, and Y. Chen, Experimental study on the effects of spray inclination on water spray cooling performance in non-boiling regime, Exp. Thermal Fluid Sci. **34**, 933 (2010).
9 W. L. Cheng, Q. N. Liu, R. Zhao, and H. L. Fan, Experimental investigation of parameters effect on heat transfer of spray cooling, Heat Mass Transfer **46**, 911 (2010).
10 T. L. Fu, Z. D. Wang, X. T. Deng, G. H. Liu, and G. D. Wang, The influence of spray inclination angle on the ultra fast cooling of steel plate in spray cooling condition, Appl. Thermal Eng. **78**, 500 (2015).
11 S. S. Hsieh, T. C. Fan, and H. H. Tsai, Spray cooling characteristics of water and R-134a. Part II: transient cooling, Int. J. Heat Mass Transfer **47**, 5713 (2004).
12 S. S. Hsieh, and S. Y. Luo, Droplet impact dynamics and transient heat transfer of a micro spray system for power electronics devices, Int. J. Heat Mass Transfer **92**, 190 (2016).
13 J. M. Tian, B. Chen, D. Li, and Z. F. Zhou, Transient spray cooling: Similarity of dynamic heat flux for different cryogens, nozzles and substrates, Int. J. Heat Mass Transfer **108**, 561 (2017).
14 Y. Li, H. Guo, Z. Zhou, Z. Zhang, X. Ma, and L. Chen, Spray morphology transformation of propane, n-hexane and iso-octane under flash-boiling conditions, Fuel **236**, 677 (2018).
15 N. Zhou, H. Feng, M. Xu, and E. Liu, Heat transfer performance and influences of spray cooling under quenching, Therm. sci. **25**, 4805 (2021).
16 M. Ciofalo, A. Caronia, M. Di Liberto, and S. Puleo, The Nukiyama curve in water spray cooling: Its derivation from temperature–time histories and its dependence on the quantities that characterize drop impact, Int. J. Heat Mass Transfer **50**, 4948 (2007).
17 M. Ebrahim, B. Elkenani, and A. Ortega, Transient surface temperatures upon the impact of a single droplet onto a heated surface in the film evaporation regime, Int. J. Heat Mass Transfer **186**, 122463 (2022).
18 K. Tsukamoto, Y. Kita, S. Inoue, T. Hamanosono, S. Hidaka, S. Ueoka, H. Fukuda, M. Kohno, and Y. Takata, On the onset of quench during spray cooling: The significance of oxide layers, Appl. Thermal Eng. **179**, 115682 (2020).
19 L. Liu, X. Wang, M. Ge, and Y. Zhao, Experimental study on heat transfer and power consumption of low-pressure spray cooling, Appl. Thermal Eng. **184**, 116253 (2021).

20 N. Zhou, H. Feng, Y. Guo, H. Chen, W. Liu, H. Peng, Y. Lei, S. Deng, and Y. Xu, Experimental study on the spray cooling heat transfer performance and dimensionless correlations for ethylene glycol water solution, Appl. Thermal Eng. **214**, 118824 (2022).

喷雾冷却的瞬态传热特性

董可为, 吴笛, 段俐, 康琦, 王佳, 刘建林, 王志伟, 段隆盛

摘要 本文搭建旋流式喷雾冷却实验系统, 研究喷雾冷却的随喷雾流态演化的瞬态传热效率. 实验观测初始温度为300 °C的高热壁面的喷雾冷却过程. 冷却工质为水, 冷却试件为铝合金方块, 面积为20 mm × 20 mm. 利用5根高精度热电偶测量冷却试件竖直方向均布5个测点的温度变化, 并结合有限差分法求解一维非稳态热传导方程, 反演获得表面热流曲线. 实验通过改变喷雾高度和喷雾流量, 得到不同工况下瞬态热流密度的演化曲线. 结果表明, 喷雾冷却过程可分为4个阶段: Ⅰ. Leidenfrost效应阶段(缓慢上升), Ⅱ. 液膜形成阶段(急剧上升), III. 沸腾阶段(逐步下降), Ⅳ. 对流蒸发阶段(趋于平衡). 冷却过程由液膜形成阶段(第Ⅱ阶段)向沸腾阶段(第III阶段)转变时, 热流密度达到峰值; 与工质压力影响相比, 喷雾高度对液膜影响作用更为显著, 5 mm喷雾高度下的换热能力要远高于10 mm及15 mm的工况, 合适的喷雾高度是促进喷雾冷却散热的重要因素.